scientific reports

Check for updates

OPEN

A multiscale approach for bridging the gap between potency, efficacy, and safety of small molecules directed at membrane proteins

Rodrigo Aguayo-Ortiz[1,5,6], Jeffery Creech[1,2,6], Eric N. Jiménez-Vázquez[1,4], Guadalupe Guerrero-Serna[1], Nulang Wang[1], Andre Monteiro da Rocha[1,2], Todd J. Herron[1,2,3] & L. Michel Espinoza-Fonseca[1]✉

Membrane proteins constitute a substantial fraction of the human proteome, thus representing a vast source of therapeutic drug targets. Indeed, newly devised technologies now allow targeting "undruggable" regions of membrane proteins to modulate protein function in the cell. Despite the advances in technology, the rapid translation of basic science discoveries into potential drug candidates targeting transmembrane protein domains remains challenging. We address this issue by harmonizing single molecule-based and ensemble-based atomistic simulations of ligand–membrane interactions with patient-derived induced pluripotent stem cell (iPSC)-based experiments to gain insights into drug delivery, cellular efficacy, and safety of molecules directed at membrane proteins. In this study, we interrogated the pharmacological activation of the cardiac Ca^{2+} pump (Sarcoplasmic reticulum Ca^{2+}-ATPase, SERCA2a) in human iPSC-derived cardiac cells as a proof-of-concept model. The combined computational-experimental approach serves as a platform to explain the differences in the cell-based activity of candidates with similar functional profiles, thus streamlining the identification of drug-like candidates that directly target SERCA2a activation in human cardiac cells. Systematic cell-based studies further showed that a direct SERCA2a activator does not induce cardiotoxic pro-arrhythmogenic events in human cardiac cells, demonstrating that pharmacological stimulation of SERCA2a activity is a safe therapeutic approach targeting the heart. Overall, this novel multiscale platform encompasses organ-specific drug potency, efficacy, and safety, and opens new avenues to accelerate the bench-to-patient research aimed at designing effective therapies directed at membrane protein domains.

Membrane proteins are pivotal players in the cell, playing essential biological roles in a variety of functions vital to the survival of organisms, including transport of ions and molecules, signal transduction across cells, serve as scaffolds to help bind the cell to a surface or substrate, and catalyze reactions in biological membranes[1,2]. Membrane proteins constitute a significant fraction (about 20–30%) of the human proteome[3], and these proteins represent more than 60% of the current drug targets[4]; enzymes, transporters, ion channels, and receptors are all common drug targets. Molecules directed at solvent-accessible pockets have been the primary strategy used to target membrane proteins[5]; indeed, virtually all therapeutics targeting membrane proteins bind to solvated regions outside the lipid bilayer[6]. Therefore, membrane protein-based drug discovery has rested on the primary assumptions that transmembrane domains are simply passive structural domains required to anchor membrane proteins to the lipid bilayer and that there are no specific sites and interactions within the transmembrane domains that can be effectively used for drug development. Recent advances in crystallography, spectroscopy and, computational biophysics now challenge this conventional view and show that transmembrane domains actively mediate functional protein–protein interactions and exert modulatory roles in membrane proteins[2].

[1]Division of Cardiovascular Medicine, Department of Internal Medicine, Center for Arrhythmia Research, University of Michigan, Ann Arbor, MI 48109, USA. [2]Frankel Cardiovascular Regeneration Core Laboratory, University of Michigan, Ann Arbor, MI 48109, USA. [3]CARTOX, Inc., 56655 Grand River Ave., PO Box 304, New Hudson, MI 48165, USA. [4]Department of Pharmacology, University of Michigan, Ann Arbor, MI 48109, USA. [5]Departamento de Farmacia, Facultad de Química, Universidad Nacional Autónoma de México, 04510 Mexico, Mexico. [6]These authors contributed equally: Rodrigo Aguayo-Ortiz and Jeffery Creech. ✉email: lmef@umich.edu

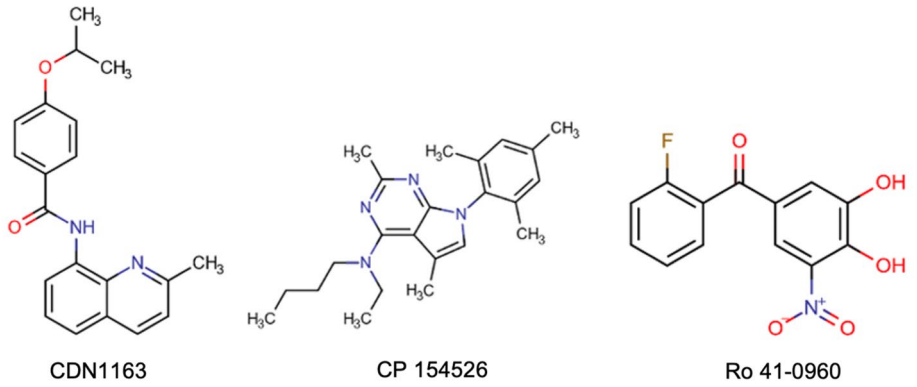

Figure 1. Structures of three activators known to target the transmembrane domain of the calcium pump.

The paradigm shift from traditional structural biology to a dynamic view of membrane proteins has enabled the discovery of effector sites located in conventionally undruggable transmembrane regions to modulate protein function[6–8]. A prime example of a druggable transmembrane protein is the cardiac sarcoplasmic reticulum Ca^{2+}-ATPase (SERCA2a). SERCA is an ATP-fueled pump that actively transports cytosolic Ca^{2+} into the sarcoplasmic reticulum during diastole in the heart, relaxing muscle cells and allowing the ventricles to fill with blood[9]. SERCA2a regulation is critical for maintaining normal heart function, and its pathological dysregulation is a hallmark of heart failure. Consequently, pharmacological stimulation of SERCA2a activity has been proposed as a therapeutic strategy to improve cardiac function[10–13]. There is extensive evidence indicating that key effector sites are localized in the transmembrane domain of the pump, including regulatory and inhibitory binding sites[14]. More recently, we have shown that the membrane protein dwarf open reading frame (DWORF) binds to the transmembrane domain of SERCA2a and directly stimulates the activity of the pump[15]. FRET-based screening assays have also demonstrated that small molecules activate SERCA2a through targeting the transmembrane domain of the pump[16]. Together, these studies illustrate the importance of SERCA2a as a pharmacological target for heart failure therapy[17,18] and a new paradigm for membrane protein-based drug discovery[13,19,20].

Membrane permeation is considered the key factor limiting the utility of chemical probes and therapeutic agents[21,22], as the suboptimal ability of molecules to penetrate the cell and engage their membrane protein target results in poor efficacy. Nonetheless, it remains unclear whether membrane permeability profiles alone are sufficiently predictive to establish the relationships between target-based potency and cell efficacy of molecules targeting membrane protein domains. Another major limitation preventing the discovery of exogenous agents that can be used as potent probes that target transmembrane protein domains is the use of heterologous expression systems to evaluate cellular efficacy. This issue is of particular importance because small-molecule screening campaigns are often performed using cells that express the foreign target in quantities suitable for high-throughput screening[23] but do not necessarily capture organ-specific cellular target engagement in and potential off-target effects[24]. Therefore, understanding the relationships between target-based potency and cell-based efficacy is of utmost importance to accelerate the discovery and development of biologically active molecules targeting transmembrane protein domains. To address this issue, here we used complementary single-molecule and ensemble-based atomistic simulations of lipid–ligand interaction, in situ enzymatic activity assays, and high-resolution optical mapping using human iPSC-derived cardiac cells to systematically interrogate pharmacological modulation of SERCA2a activation as a model. The result is a comprehensive platform that encompasses drug delivery, target engagement, cellular efficacy, and safety of molecules directed at membrane proteins.

Results and discussion

Target-based potency of small molecules directed at cardiac SERCA2a. In this study, we used only three known allosteric activators directed at the transmembrane domain of SERCA2a (Fig. 1). CDN1163 was reported to activate the housekeeping SERCA2b isoform[25], whereas compounds CP-154526 and Ro 41-0960 have been shown to activate cardiac SERCA2a isoform[16]. It is important to note that other small molecules have been reported to activate SERCA2a; however, these effects are indirect (i.e., through phospholamban binding[26], and only CDN1163, CP-154526, and Ro 41-0960 have been characterized as direct SERCA activators[16,25,26]. Therefore, we first evaluated the activity of these molecules directed at SERCA2a in cardiac sarcoplasmic reticulum (SR) microsomes isolated from hearts using an NADH-coupled ATPase assay. These ATPase activation assays confirmed that all three molecules stimulate SERCA2a activity with mean half-maximum effective concentration (EC_{50}) values between 0.8 and 27 μM (Table 1). These findings indicate that these molecules are relatively potent toward SERCA2a, with average EC_{50} values in the low μM range. The small molecules also increase ATPase turnover (V_{max}) by 27–38% at a Ca^{2+} concentration of 10 μM (Table 1); these findings suggest that these SERCA activators stimulate maximal Ca^{2+} uptake rates in cardiac SR microsomal preparations. Together, these findings support previous studies and demonstrate that molecules CDN1163, CP-154526, and Ro 41-0960 are direct activators of the cardiac SERCA2a pump.

Compound	EC_{50} (μM)[a]	ΔV_{max} (%)[a]	$LogP_{BLM}$[b]	ΔG_{bind} neutral (kcal mol^{-1})[c]	ΔG_{bind} ionized (kcal mol^{-1})[c]
CDN1163	1.6 ± 0.3	27 ± 3	2.3	− 3.4	–
CP-154526	0.8 ± 0.4	31 ± 4	5.6	− 8.3	− 5.1
Ro 41-0960	27 ± 1.3	38 ± 2	− 5.9	− 8.8	− 4.8

Table 1. Half-maximum effective concentration (EC_{50}), change in ATPase turnover (V_{max}), partition coefficient, and ligand–lipid free energy of binding of SERCA activators. [a]Values were obtained from in situ SERCA2a ATPase activity experiments ($n = 3$); values are reported as mean ± SEM. [b]$LogP_{BLM}$ is the permeability coefficient of molecules through the black lipid membrane. [c]Estimated from the PMF profile of the umbrella sampling calculations.

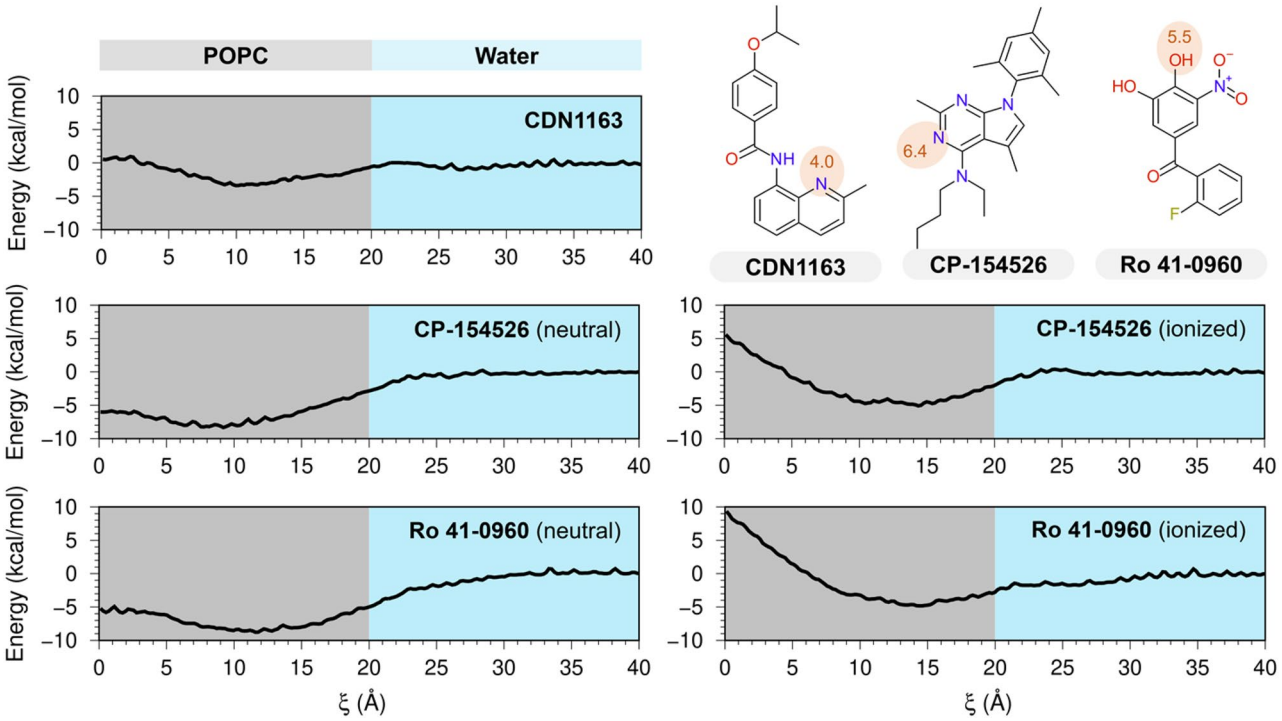

Figure 2. Bilayer-crossing free energy profiles of SERCA2a activators. Profiles are represented by the potential of the mean force (PMF) of SERCA2a activators CDN1163, CP-153526, and Ro 41-0960 along the normal z-axis of a POPC membrane; the distance along the z-axis was used here as a reaction coordinate (ξ). The chemical structures in the upper right indicate the location of titratable groups and their corresponding pKa values (red circles); based on these pKa values, Bilayer-crossing free energy profiles were calculated for either neutral or ionized states of the small molecules. The gray area illustrates only one leaflet of the lipid bilayer.

Bilayer crossing profiles of SERCA2a activators. Upon establishing the target-based potency of the three activators toward SERCA2a, we used atomistic simulations to evaluate the bilayer-crossing free energy profiles of these molecules. We predict that at physiological pH of 7.1–7.2[27], CDN1163 is neutral (pKa = 4.0). Conversely, a pKa value of 6.4 calculated for CP-154526 ($pK_a = 6.4$) suggests that this molecule could be either neutral or ionized, whereas Ro 41-0960 ($pK_a = 5.5$) is predominantly charged at physiological pH. Based on these pK_a calculations, we computed the POPC bilayer-crossing free energy profiles of the CDN1163 and CP-154526 in their neutral state, and Ro 41-0960 in its ionized state. Additionally, we calculated the free-energy profiles for charged CP-154526 and neutral Ro 41-0960 to account for the uncertainty of the model (Root-mean-square error of 1.1 pKa units)[28]. The profiles in Fig. 2 highlight the range of energetic barriers possible with different SERCA2a activators and ionization states, with all the umbrella sampling windows provided in Supplementary Fig. S1 (Supplementary Information). All electrically neutral molecules have a small membrane entry barrier from the solution (Fig. 2), but the energy barrier is not considerably affected by ionization, as observed in the bilayer-crossing free energy profiles of electrically charged CP-154526 and Ro 41-0960 (Fig. 2). After crossing this energetic barrier, the compounds reach their preferred penetration depth, either close to the lipid headgroup or the membrane midplane (Fig. 2). Except for the ionized states of CP-154526 and Ro 41-0960, there is a peak for the free energy profile at the center of the bilayer representing the energetic cost of burying the molecules within the bilayer center. Despite these differences, all molecules interact favorably with the lipid bilayer regardless of their ionization state, with free energies of binding (ΔG_{bind}) between − 3.4 and − 8.8 kcal mol^{-1} (Table 1).

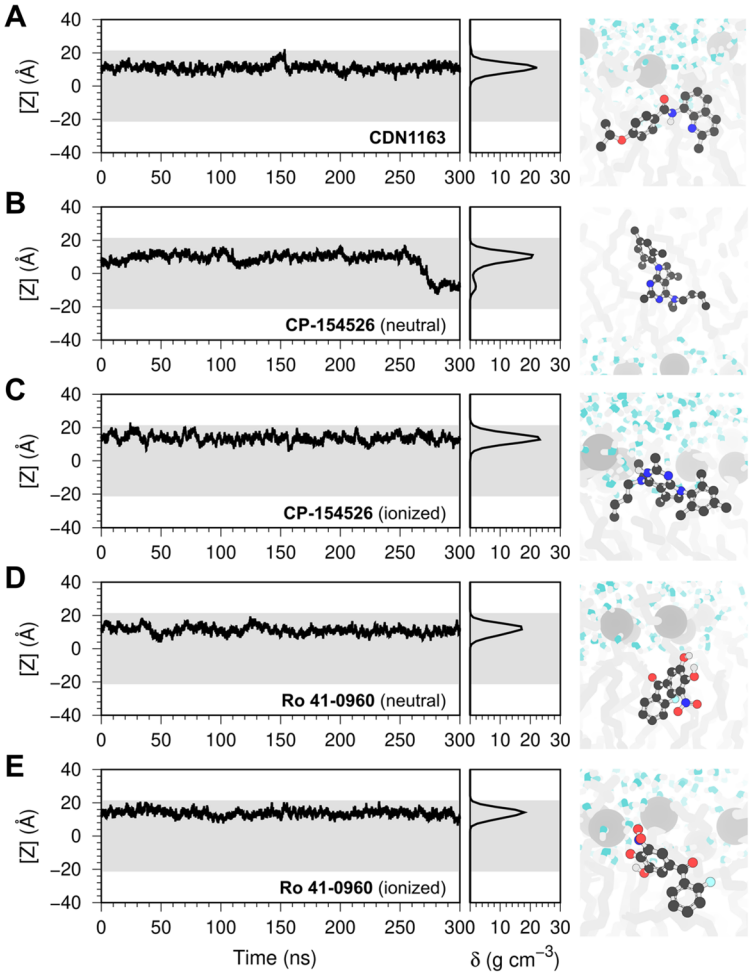

Figure 3. Single-molecule atomistic simulations of ligand–membrane interactions. The plots represent the position of a single molecule of (**A**) CDN1163, (**B**,**C**) CP-154526, and (**D**,**E**) Ro 41-0960 bound to a solvated POPC membrane. We show the time-dependent position of the molecule along the z-axis of the lipid–water system (left), the relative density (δ) profile of the molecules in the lipid bilayer (center), and the orientation of the molecules in the lipid bilayer extracted at the end of the trajectories (right). In all plots, the shaded area represents the location of the lipid bilayer. The small molecules are shown as ball and stick representation; lipid headgroups and tails are shown as light gray spheres and sticks, respectively; water molecules are shown as white and blue sticks.

More importantly, we found that Ro 41-0960 has a high affinity for the lipid bilayer, in contrast to the predicted negative logP calculated for this molecule (Table 1).

Single-molecule simulations of ligand–membrane interactions. We performed unrestrained molecular dynamics (MD) simulations of the activators embedded in a POPC bilayer as a complementary approach to evaluate the stability of the ligand–membrane interactions. Figure 3 shows the time-dependent and probability distribution of the vertical position of the molecules in the lipid bilayer, where [Z] = 0 Å denotes the membrane center of mass. In agreement with the bilayer-crossing free energy profiles, unrestrained MD simulations show that the molecules remain bound to the lipid bilayer and localize at the interface between the polar and nonpolar regions of the membrane, e.g., near or below the headgroups of POPC (Fig. 3). The vertical position of the molecules is determined by the charge of the compounds: electrically neutral molecules penetrate deeper into the membrane at distances between 9 and 12 Å from the membrane center of mass, whereas charged molecules localize farther from the center of the lipid bilayer (Fig. 3). For example, CDN1163 binds about 9 Å away from the center of the bilayer, while Ro 41-0960 maintains an average distance of 14 Å from the center of mass of the POPC bilayer and can further localize into the headgroup-water interface (e.g., at $t = 25–35$ ns, Fig. 3). The unrestrained MD simulations correlate well with PMF calculations and show that both electrically neutral and charged states of Ro 41-0960 remain bound to the lipid bilayer despite carrying a charged nitro group. The qualitative and quantitative agreement between biased and unbiased atomistic simulations implies that these activators interact favorably with a lipid bilayer. The affinity of these molecules for the lipid bilayer

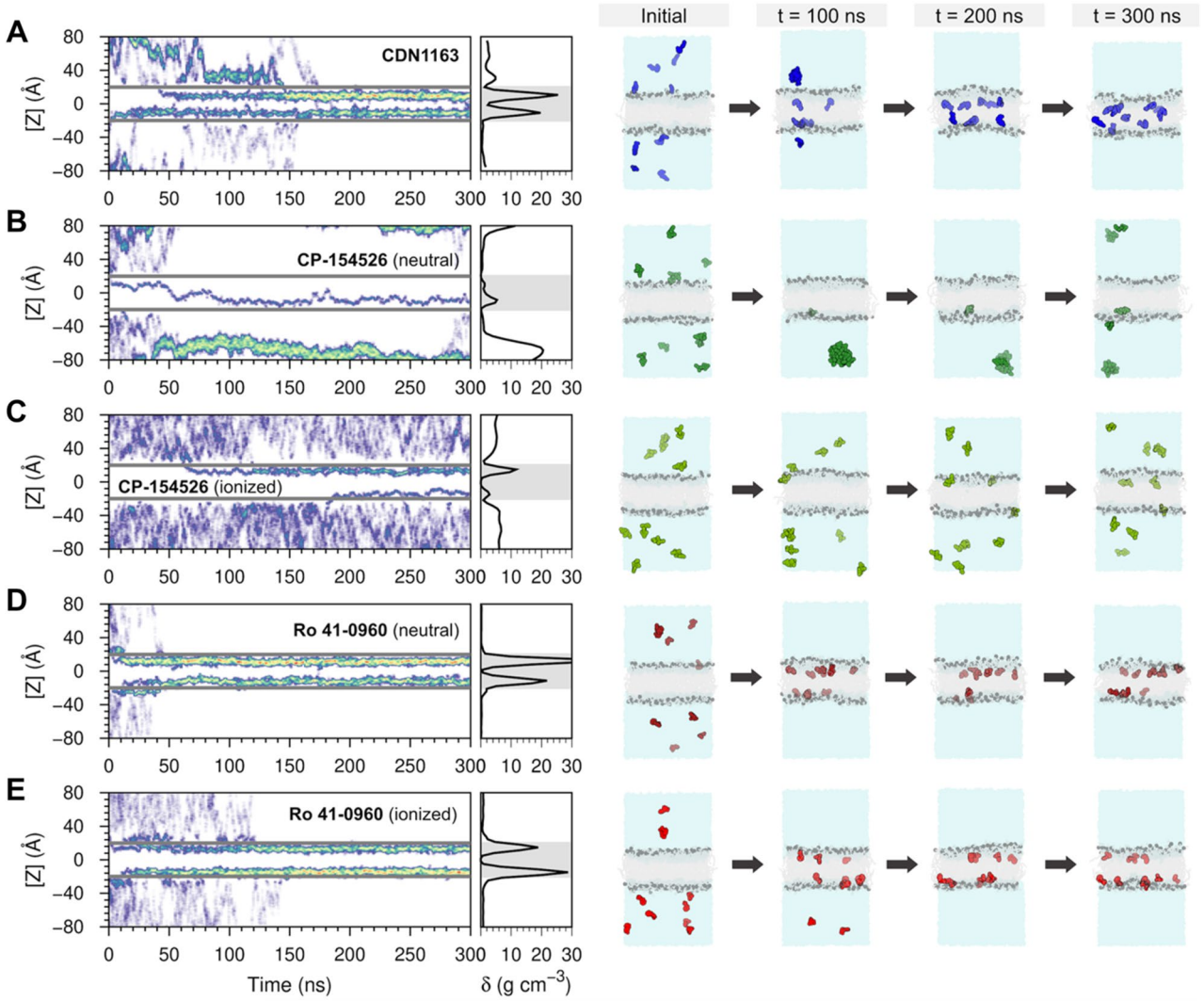

Figure 4. Ensemble-based atomistic simulations of ligand–membrane interactions of SERCA2a activators. The left panels show the time-resolved behavior of SERCA2a activators in a lipid–water environment and the relative density profiles of SERCA2a activators in a lipid–water system obtained from the ensemble-based MD simulations. The figure shows the position of the molecules relative to the z-axis of the system (left) and the relative density (δ) profile (right) calculated for (**A**) CDN1163, (**B**,**C**) CP-154526, and (**D**,**E**) Ro 41-0960. The gray horizontal lines (left) and the shaded area (right) represent the boundaries of the lipid bilayer. We show time-dependent configurations of each system containing a solvated membrane and ten copies of each SERCA2a actiator. The simulations capture spontaneous insertion of small molecules into the membrane as well as ligand–ligand interactions during the 300 ns of simulation time. CDN1163 (blue), CP-154526 (green), and Ro 41-0960 (red) are shown as spheres; lipids and water molecules are shown in gray and blue, respectively.

supports the concept that these effectors activate SERCA2a by interacting with the transmembrane domain of the protein.

In addition to the localization in the lipid bilayer, another important variable to consider is the translocation of the small molecules across the membrane. This is especially important for targets localized in intracellular compartments, including the sarcoplasmic reticulum where SERCA2a is found. Lipid-bilayer crossing free-energy profiles show that electrically neutral CP-154526, Ro 41-0960, and to a certain extent CDN1163 can translocate freely across the lipid bilayer. Analysis of the unbiased MD trajectories showed that electrically neutral CP-154526 undergoes a single spontaneous exchange event between membrane leaflets (i.e., at $t = 275$ ns, Fig. 3). Although the PMF profiles of electrically neutral Ro 41-0960 and CDN1163 indicate that these molecules can cross the membrane, we did not observe leaflet exchange of this molecule in the timescales studied here.

Ensemble-based atomistic simulations of ligand–membrane provide unique insights into ligand–membrane interactions. We performed ensemble-based MD atomistic simulations[29] as a complementary approach to better capture the behavior of SERCA2a activators in a lipid–water environment and in real-time. We found that the ensemble-based simulations capture the spontaneous insertion of small molecules into the membrane (Fig. 4) observed in the single-molecule trajectories. For example, the maximum relative

density of CDN1163 in the lipid bilayer occurs at 11–12 Å from the center of the bilayer, whereas electrically charged Ro 41-0960 resides primarily at ~ 14 Å from the center of the bilayer (Fig. 4). The relative density profiles of the CP-154526, especially in its electrically charged state, are also in good qualitative and quantitative agreement with unbiased single-molecule MD simulations (Fig. 3). The reproducibility of ligand–membrane interactions across different MD approaches validates the ensemble-based simulations as an approach to gain further insights into the behavior of small molecules in a lipid–water environment.

While the ensemble-based and single molecule-based trajectories are in general quantitative and qualitative agreement, the former revealed unique differences in the ligand–ligand and ligand–protein profiles among SERCA2a activators. We found that the 10 molecules of CDN1163 simulated in the lipid–water system bind to the lipid bilayer at t = 170 ns and remain bound to the membrane for the remainder of the simulation time (Fig. 4A). In contrast with the favorable ligand–lipid interaction single-molecule profiles of CP-154526 (Figs. 1, 2), ensemble-based simulations showed that this molecule has a strong preference for the aqueous phase of the system (Fig. 4B,C). Surprisingly, the preference for the aqueous phase is more pronounced in the electrically neutral state of the molecule, where only 10–20% of the CP-154526 molecules transfer to the lipid bilayer (Fig. 4B). More importantly, we found that electrically neutral CP-154526 aggregates in the aqueous phase (Fig. 4B), although ionization partially mitigates this effect (Fig. 4C). Finally, MD simulations of Ro 41-0960 showed that all 10 molecules bind to the lipid bilayer at t = 40 ns for the electrically neutral molecule and t = 140 ns for the electrically charged form of the ligand; as in CDN1193, Ro 41-0960 remains bound to the lipid bilayer in both trajectories. We found that this behavior is consistent across ionization states, thus indicating that changes in ionization state do not affect the ability of Ro 41-0960 to associate with the lipid bilayer.

In addition to the differences in ligand–ligand and ligand–lipid interactions observed in the ensemble-based simulations, a notable discovery made here is the clear differences in ligand translocation profiles across the lipid bilayer that are not entirely captured by single-molecule simulations. Specifically, the density profile of CDN1163 shows an increase in the relative density of this molecule around the center of the lipid bilayer ($[Z] = 0$ Å, Fig. 4A), suggesting that this molecule penetrates across the lipid bilayer in the time scales used in this study. Similarly, electrically neutral CP-154526 penetrates across the membrane; penetration occurs only once in the trajectory, which is explained by the preference of this molecule to partition into the aqueous phase. Conversely, the relative density of the small molecules around the center of the lipid bilayer is nearly 0 g cm^{-3} in the trajectories of electrically charged CP-154526 as well as Ro 41-0960 (charged and neutral), thus indicating that these molecules do not penetrate across the lipid bilayer in the MD trajectories (Fig. 4D,E).

Cell-based efficacy of SERCA2a activators in human iPSC-derived cardiac cells. We determined the effects of these molecules on Ca^{2+} flux dynamics and beating rate in spontaneously beating human iPSC-derived cardiomyocytes using high-resolution optical mapping. We found that the human iPSC-derived cardiomyocytes used in this study are ideally suited for studying the pharmacological stimulation of SERCA2a because they express the major components involved in Ca^{2+} handling, including SERCA2a, the ryanodine receptor (RyR); the voltage-dependent L-type Ca^{2+} channel, α-1C subunit ($Ca_v1.2$); the cardiac Na^+–Ca^{2+} exchanger (NCX1); and phospholamban (PLN) (Fig. 5A). In response to β2-adrenergic stimulation, these iPSC-derived cardiac cells populate phosphorylated phospholamban, the main regulator of SERCA2a activity in the heart. This pharmacological effect in response to treatment of iPSC-derived cardiac cells with isoproterenol is illustrated in Fig. 5B.

We first determined the effects of CP-154526, CDN1163, and Ro 41-096 at six different concentrations on the rise and decay in cytosolic Ca^{2+}, i.e., the Ca^{2+} transient amplitude. We compared these effects to those induced by isoproterenol, which has both positive inotropic and chronotropic effects on the cardiomyocyte via adrenergic stimulation.

CP-154526 at concentrations of 0.5, 1, 5, and 10 μM increases the amplitude of the Ca^{2+} transient similar to that induced by isoproterenol; however, CP-154526 has a significantly lower effect on the Ca^{2+} transient amplitude at concentrations of 0.1 and 50 μM (Fig. 6A, left panel). We found no significant differences in the Ca^{2+} transient amplitude between CDN1163 at all six concentrations and isoproterenol (Fig. 6A, middle panel). In contrast, the changes in the Ca^{2+} transient amplitude induced by Ro 41-0960 are significantly smaller than those produced by isoproterenol (Fig. 6A, right panel).

Next, we measured the changes in Ca^{2+} transient duration at 50% recovery ($CaTD_{50}$) to determine whether the SERCA2a activators tested here operate as lusitropic agents that accelerate the Ca^{2+} transient decay in human iPSC-derived cardiomyocytes. We found that the decrease in the $CaTD_{50}$ induced by the three compounds at all concentrations is significantly different from that induced by isoproterenol (Fig. 6B). These differences are not surprising because CP-154526, CDN1163, and Ro 41-096 are expected to act primarily upon SERCA2a activation, whereas isoproterenol is a positive inotrope[30] that regulates the function of SERCA2a and other cardiac Ca^{2+} handling proteins (e.g., the $Ca_v1.2$ voltage-gated calcium channels[31]) via adrenergic stimulation. Nevertheless, we found important differences in $CaTD_{50}$ across all three SERCA2a activators. Specifically, we found that different concentrations of CP-154526 and Ro 41-0960 induce effects on the $CaTD_{50}$ that are substantially different from those produced by isoproterenol (Fig. 6B). For instance, both CP-154526 and Ro 41-0960 increase the duration of the Ca^{2+} transient at a compound concentration of 5 μM, whereas a shortening of the Ca^{2+} transient is produced by high concentrations (> 50 μM) of Ro 41-0960 (Fig. 6B, right panel). Conversely, our optical mapping experiments indicate that CDN1163 shortens the duration of the Ca^{2+} transient at most of the concentrations tested in this study (0.5–50 μM, Fig. 6B, middle panel).

Lastly, we determined the effects of all compounds on the changes in the beat rate (i.e., chronotropy) of human iPSC-derived cardiomyocytes. In all cases, there are significant differences in the changes in chronotropy induced by the compounds compared to the inotrope isoproterenol. However, we found that the beat rate of

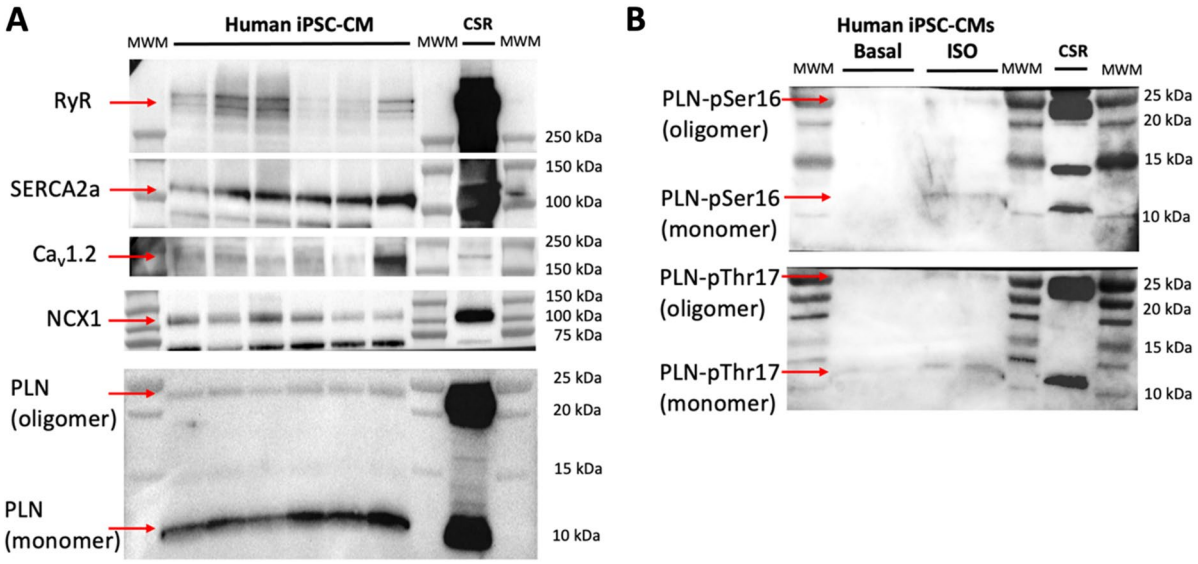

Figure 5. Expression of major Ca^{2+} handling proteins in human iPSC-derived cardiomyocytes by western blot analysis. (**A**) Western blot analysis of human cardiomyocytes showed that these cells express all major proteins involved in Ca^{2+} transport and regulation of the cardiac calcium pump SERCA2a. We analyzed the expression of the following proteins: RyR, ryanodine receptor; SERCA2a, the cardiac isoform of sarcoplasmic reticulum Ca^{2+}-ATPase; $Ca_v1.2$, voltage-dependent L-type Ca^{2+} channel, α-1C subunit; NCX1, Na^+–Ca^{2+} exchanger; PLN, phospholamban. (**B**) Detection of phosphorylated phospholamban (PLN) at positions Ser16 (PLN-pSer16) and Thr17 (PLN-pThr17) in response to pharmacological β2-adrenergic stimulation with isoproterenol (ISO, 1 μM); untreated cells were included in the analysis (basal, negative control). In all cases, we used a pig heart membrane preparation as a control ('CSR' lane) for the expression of Ca^{2+} handling proteins tested in this study.

human iPSC-derived cardiomyocytes is unaltered by CDN1163 and Ro 41-0960 (Fig. 6C). Nevertheless, a comparison between CDN1163 or Ro 41-0960 and CP-154526 showed that this compound has a significant effect on chronotropy ($p < 0.05$), increasing the beat rate of cardiac cells by 16–33% at compound concentrations of 0.1, 5, 10, and 50 μM (Fig. 6C, left panel).

Atomistic simulations and cell-based experiments bridge the gap between potency and efficacy of activators targeting SERCA2a. How do simulations and experiments integrate to bridge the gap between target-based potency and efficacy of bioactive molecules directed at SERCA2a in cardiac cells? To answer this question, it is instructive to pick two similar examples: CDN1163 and CP-154526 activate SERCA2a in situ with similar μM potency, yet these molecules produce different effects in human iPSC-derived cardiac cells. More specifically, only CDN1163 activates SERCA2a in the cardiomyocyte, as reflected by the ability of small molecules to increase the Ca^{2+} transient amplitude and decrease the $CaTD_{50}$ without significant effects on the chronotropy of the healthy cardiomyocyte[13,32]. Here, the atomistic simulations provide a mechanistic explanation for these differences: both molecules can penetrate across the membrane (Fig. 2), but CDN1163 predominantly binds to the lipid bilayer while CP-154526 partitions to the aqueous phase of the lipid–water system (Fig. 4). Functional evaluation on human iPSC-derived cardiomyocytes complements the MD-based results and provides a mechanistic hypothesis for the differences between the pharmacological effects of the SERCA2a activators studied here. For instance, the increase in the amplitude of the Ca^{2+} transient, the prolongation of the Ca^{2+} transient decay, and changes in chronotropy observed in response to CP-154526 might result from several factors, including interactions with soluble proteins involved in Ca^{2+} dynamics[33,34] and uncoupling of the SERCA-mediated ATP hydrolysis from Ca^{2+} transport.

This complementary approach also explains the effects of Ro 41-0960 on the cardiomyocyte: in a lipid–water environment, this molecule partitions primarily to the lipid bilayer, in agreement with the ability of this protein to bind to the transmembrane domain of SERCA and activate it in an isoform-specific manner[16]. However, atomistic simulations showing that Ro 41-0960 permeates poorly across the cell membrane, thus translating into poor delivery to the sarcoplasmic reticulum and insufficient SERCA2a-mediated lusitropic effect in human iPSC-derived cardiac cells. In summary, the differences in cell-based efficacy may be attributed to a combination of suboptimal ligand delivery to the lipid bilayer, as detected by our MD simulations, as well as off-target effects, as suggested by our cell-based screening assays. Based on this evidence, we can conclude that among the molecules studied here, only CDN1163 targets and activates SERCA2a in human iPSC-derived cardiac cells.

We note that while these simulations alone cannot provide direct insights into the specific interactions between SERCA2a and its activators, the MD simulation pipeline proposed here is complementary to structure-based studies to streamline the selection of hit candidates targeting membrane domains early in the drug discovery campaigns. It is also important to note that while CP-154526 and Ro 41-0960 do not produce the expected pharmacological effects on human iPSC-derived cardiac cells, the high-throughput screening campaigns that led to the discovery of these molecules are not 'wrong'[16], because these molecules are actual activators of

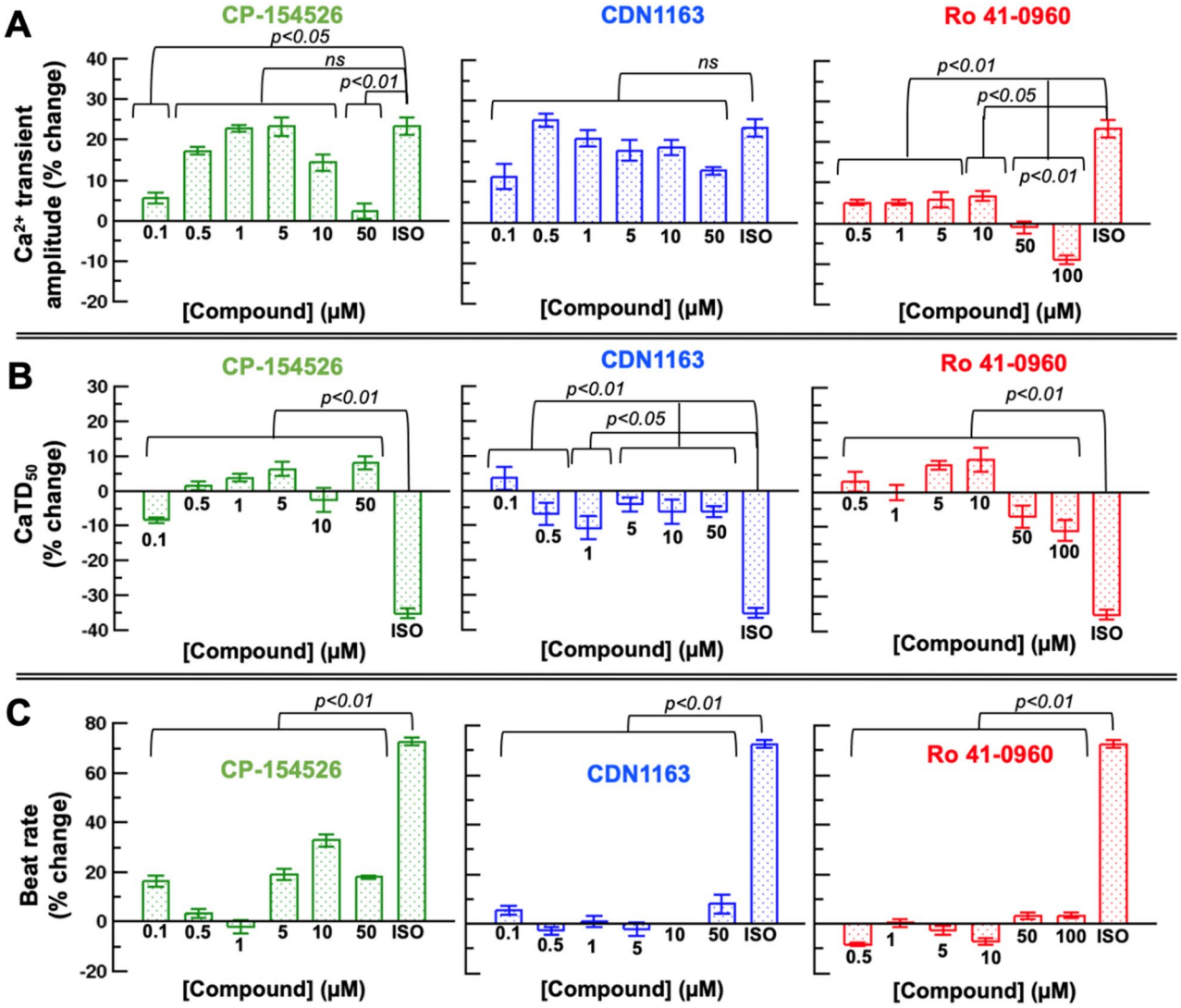

Figure 6. Functional characterization of SERCA2a activators in human iPSC-derived cardiomyocytes. Concentration-dependent effects of SERCA2a activators CP-154526, CDN1163, and Ro 41–0960 on (**A**) the Ca^{2+} transient amplitude, (**B**) the Ca^{2+} transient duration at 50% recovery ($CaTD_{50}$), and (**C**) beat rate in normal human iPSC-derived cardiomyocytes. We compared these effects to those induced by isoproterenol (ISO), which has both positive inotropic and chronotropic effects on the cardiomyocyte. Results are expressed as percent change from baseline values in Hank's balanced salt solution and reported as mean ± SEM ($n = 6$). Groups were compared using a one-way analysis of variance (ANOVA) with the Dunnett test.

SERCA2a in situ (Table 1). Instead, these molecules can be integrated into future structure–activity campaigns aimed at elucidating transmembrane effector sites that can be targeted for therapeutic modulation, designing new chemical probes with optimal potency, and cell-based efficacy, and dissecting the molecular mechanisms underlying small-molecule SERCA activation[14]. Achieving these goals will ultimately enable advance therapeutic interventions that directly target the molecular basis of the disease in the failing heart[35].

Pharmacological activation of SERCA2a does not induce pro-arrhythmogenic events in human iPSC-derived cardiac cells. Finally, we addressed drug-induced cardiac toxicity, an issue of significant concern in drug discovery trials, particularly when a promising new lead has a desired pharmacological effect that occurs at the expense of long-term pro-arrhythmia cardiotoxicity[36,37]. Hence, an important question we ask here is whether pharmacological activation of SERCA2a may induce Ca^{2+}-dependent changes in excitability that lead to arrhythmogenic currents originating from the overload of SR with Ca^{2+} in response to sustained stimulation of the pump[38]. To rule out this effect, we performed drug-induced cardiotoxicity screening using high-resolution optical mapping with a voltage-sensitive dye to test the effects of CDN1163 on conduction velocity (CV, Fig. 7A) and action potential duration at 90% repolarization (APD_{90}) in spontaneously beating human iPSC-derived cardiac cells (Fig. 7B). We found that neither CV nor APD_{90} was significantly affected by the treatment of cardiomyocytes with the SERCA activator CDN1163. Specifically, we found that the CV was 17.5 ± 5 cm/s for

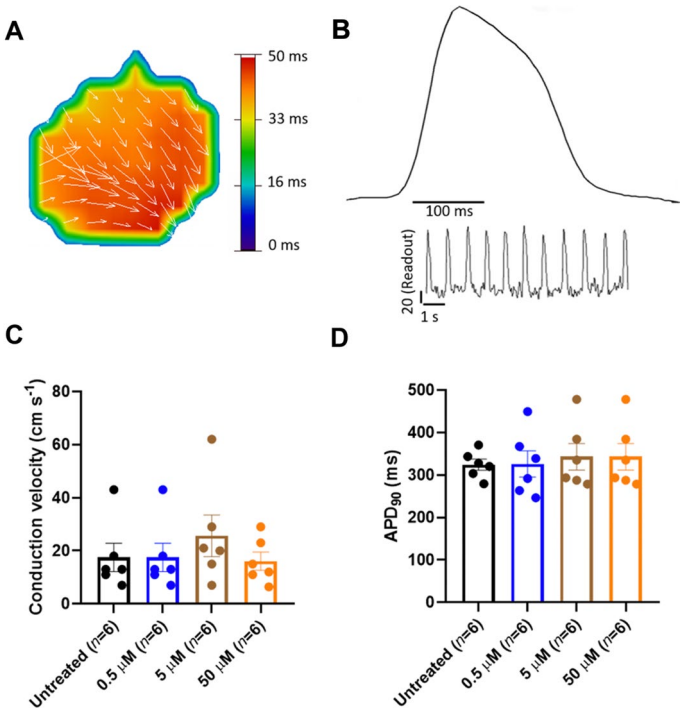

Figure 7. Conduction velocity and APD_{90} after treatment of human iPSC-derived cardiomyocytes with the SERCA activator CDN1163. (**A**) Representative impulse propagation during the spontaneous activity of untreated monolayer syncytium formed of human iPSC-derived cardiac cells. Impulse propagation is represented by the activation maps of action potential propagation at different activation times, with the arrows showing the direction of the propagation wave across the monolayer syncytium. (**B**) Representative trace of the spontaneous action potential (AP) obtained by optical mapping of a syncytium formed by human iPSC-derived cardiomyocytes. The inset represents single-pixel signals of spontaneous optical AP recordings. (**C**) Conduction velocity (CV) calculated from each activation map in the presence and absence (untreated control) of CDN1163. We found no significant changes in CV between the control and treatment groups. (**D**) Quantification of APD_{90} from optical mapping readings shown in panel (**B**). We found that treatment of human iPSC-derived cardiomyocytes with CDN1163 does not have significant effects on the APD90 compared to the untreated control. Data are reported as mean ± SEM ($n = 6$). Groups were compared using a one-way analysis of variance (ANOVA) with the Dunnett test; statistical significance was set at $p < 0.05$.

untreated cells compared to 19.3 ± 4 cm/s, 25.6 ± 8 cm/s, and 16 ± 3 cm/s for treatment of cells with 0.5, 5 and 50 μM concentrations of CDN1163, respectively (Fig. 7C). Interestingly, we found that the CV is not compromised in electrically coupled iPSC-CMs monolayer syncytia even at very high concentrations of the compound. Furthermore, the APD_{90} values were similar in all experimental conditions: 324.2 ± 13 ms for untreated cells; and 326.2 ± 31 ms, 342.9 ± 31 ms, and 344.2 ± 24 ms for monolayer syncytia treated with CDN1163 at concentrations of 0.5, 5, and 50 μM, respectively (Fig. 7D). Altogether, the data give us an idea that the compound CDN1163 is not leading to significant electrical alterations in iPSC-derived cardiomyocytes. These findings are important because changes in CV and/or APD_{90} are associated with pro-arrhythmia effects, such as re-entrant excitation or early/delayed after depolarizations[37,39,40]. Therefore, our data indicate that pharmacological stimulation of SERCA2a activity using a relatively potent activator does not induce pro-arrhythmogenic effects in human iPSC-derived cardiac cells. These findings are complementary to previous studies that have shown that stimulation of SERCA2a activity has anti-arrhythmic properties via negative feedback for the Ca^{2+} wave generation and propagation[41]. These studies illustrate the importance of integrating organ-specific safety studies earlier into both physiology studies and drug discovery pipelines aimed at validating the use of membrane proteins as safe therapeutic targets.

Conclusion

In summary, we studied small-molecule activation of SERCA2a in human cardiomyocytes to explain the relationships between target-based potency and cell-based efficacy of bioactive molecules targeting a transmembrane protein domain. This approach, which integrates atomistic simulations and high-resolution experiments using human iPSCs, provides a vivid picture of cellular drug delivery and target engagement of molecules directed at membrane proteins. The significance of this approach is illustrated by its potential to distinguish and explain direct target engagement *vs* off-target effects early in the drug discovery process, as well as its broad applicability to a variety of organ- and patient-specific human cell lines[42,43], to more complex multicomponent lipid bilayer mixtures (i.e., those that closely match the lipid composition of the membrane), and complementary experimental

and computational tools[44–46]. The result is a powerful platform to accelerate the discovery and design of bioactive molecules with well-defined potency and cell permeability that can be applied for the systematic interrogation and pharmacological modulation of membrane protein function. We anticipate that this pipeline is complementary to structure-based studies to streamline the selection of hit candidates targeting membrane domains early in the drug discovery campaigns. The flexibility of this platform to use iPSC allows it to expand into the areas of precision medicine, as it allows the use of patient-derived disease cell lines and their gene-corrected isogenic controls for evaluating the therapeutic efficacy and safety of molecules targeting transmembrane protein domains[47].

Materials and methods

Setup of small molecules and prediction of LogP values. The 3-D structures of SERCA2a activators CDN1163 (CID: 16016585), CP-154526 (CID: 5311055), and Ro 41-0960 (CID: 3495594) were retrieved from the PubChem database (https://pubchem.ncbi.nlm.nih.gov)[48]. Geometry optimization was performed using the MMFF94s force field implemented in the *obminimize* module of OpenBabel[49]. We employed the chemicalize tool developed by ChemAxon[50,51] to predict the pK_a of the three molecules. The passive translocation of each of the compounds across a lipid bilayer of 1,2-dioleoyl-*sn*-glycero-3-phosphocholine at 300 K and pH 7.1 was carried out with the PerMM server[52] using "Drag" method to calculate the pathway. We assigned the pKa values and the charge at neutral pH in the PDB header of compounds CP-154526 ($pK_a = 6.37$, basic N atom) and Ro 41-0960 ($pK_a = 5.54$, acidic oxygen atom). From this calculation, we retrieved the permeability coefficient of molecules through the black lipid membrane ($logP_{BLM}$).

Bilayer-crossing profiles of SERCA2a activators. Umbrella sampling simulations were carried out across a 1-palmitoyl-2-oleoyl-*sn*-glycero-3-phosphocholine (POPC) membrane for each of the compounds with the AMBER99SB-ILDN force field[53] implemented in GROMACS 5.1.4[54]. For this study, we chose POPC as a lipid model because this lipid is predominantly found in the membrane of both the sarcolemma and the SR membrane in muscle cells[55,56], and therefore we anticipate that this lipid composition recapitulates both membrane permeability and retention across both the sarcolemma and the SR. Ligand topologies and parameters were generated with the ACPYPE interface[57] using AM1-BCC method to compute partial charges. POPC lipid parameters were taken from the Slipids (Stockholm Lipids) force field[58]. For the system setup, we set the molecules approximately 4.0 nm away from the center of mass of a pre-equilibrated lipid bilayer comprised of 100 POPC molecules. The system was solvated using the TIP3P water model and neutralized with sodium and chloride ions. Energy minimization and equilibration using NVT and NPT ensembles (1 ns e/a) were carried out restraining the initial position of the molecule in the aqueous solution. The equilibrated systems were further used to pull the compound into the center of the POPC lipid bilayer during 500 ps with a pulling rate of 0.01 nm ps^{-1} and a harmonic force constant of 500 kJ mol^{-1} nm^{-2}. The pulling simulation was performed at 310 K and 1.0 bar using the Nosé–Hoover thermostat[59] and the semi-isotropic Parrinello–Rahman barostat[60]. Forty-three to forty-six configurations were selected along the z-axis reaction coordinate (ξ) for the umbrella sampling simulations. Each configuration was energy minimized and submitted to a restrained NPT equilibration before 10-ns of NPT production run, applying a harmonic force constant of 1000 kJ mol^{-1} nm^{-2} to the compound. The position and force data of all the configurations were evaluated with the Weighted Histogram Analysis Method (WHAM)[61] to generate the potential of mean force (PMF) profile. The snapshot with the lowest energy in the PMF profile of each compound was submitted to 300 ns non-restrained NPT production runs at 310 K and 1.0 bar using the previously described thermostat and barostat algorithms. The density profiles were computed with the *density* built-in tool of GROMACS 5.1.4, while the center of mass position of the molecule in the z-axis of the membrane was calculated with MDAnalysis python library[62].

Ensemble-based MD simulations of unbound molecules in a lipid–water environment. A total of 10 molecules of each compound, to a final concentration of ~ 17 μM, were randomly placed in the water phase of a system containing a POPC lipid bilayer consisting of 250 lipid molecules and about 34,300 water molecules. The system was energy minimized and equilibrated during 1 ns using NVT and NPT ensembles. The equilibrated system was subsequently submitted to 300 ns NPT production run using the previously described parameters. Graphs were made using Gnuplot 5.0[63]; visualization was performed using PyMOL version 1.7[64].

Obtention of cardiac muscle sarcoplasmic reticulum microsomes containing SERCA2a. Pig hearts were obtained post-mortem from a near abattoir and placed in ice-cold 10 mM $NaHCO_3$. Ventricular tissue was isolated, minced, and homogenized with a Waring immersion blender in 5 volumes of 10 mM $NaHCO_3$ at 4 °C. All procedures were done at 4 °C and all the buffers contained protease inhibitors (Sigma, St. Louis, MO, USA). The homogenate was centrifuged at 6500*g* for 20 min. The supernatant was filtered through 6 layers of gauze and centrifuged at 14,000*g* for 30 min. The supernatant was filtered and centrifuged at 47,000*g* for 60 min. The pellet was resuspended in a buffer containing 0.6 M KCl and 20 mM Tris (pH = 6.8) using a Teflon Potter–Elvehjem homogenizer. The suspension was then centrifuged at 120,000*g* for 60 min. The pellet obtained was resuspended and homogenized in a solution containing 0.3 M sucrose and 5 mM HEPES (pH 7.4). The protein concentration of the microsomal suspension was determined by using Coomassie Plus assay kit (Thermo Fisher Scientific, Waltham, MA, USA) in a Synergy H1 multi-mode plate reader (BioTek, Winooski, VT, USA).

Measurement of SERCA2a ATPase activity. Concentration-dependent SERCA2a activation assays of CD1163, CP-154526, and Ro 41-0960 (Sigma-Aldrich, St. Louis MO, USA) were performed using microsome preparations obtained from fresh pig hearts. An enzyme-coupled NADH-linked ATPase assay was used to measure SERCA2a ATPase activity in 96-well microplates. Each well-contained assay mix (50 mM MOPS, pH 7.0),

100 mM KCl, 5 mM $MgCl_2$, 1 mM EGTA, 0.2 mM NADH, 1 mM phosphoenolpyruvate, 10 IU/mL of pyruvate kinase, 10 IU/mL of lactate dehydrogenase, and 1 µM of the calcium ionophore A23187 (Sigma-Aldrich, St. Louis, MO, USA), and added $CaCl_2$ to set the free Ca^{2+} concentration to 10 µM. The Ca^{2+}-dependent concentration–response effects of these molecules have been reported in previous studies[16,25]. Based on these studies, here we used a Ca^{2+} concentration of 10 µM because it recapitulates the limiting activity of SERCA2a at high Ca^{2+}. 4 µg/mL of microsomal preparation, $CaCl_2$, compound, and assay mix were incubated for 20 min. We tested activity at 11 different concentrations of the compound in the range of 0.05–50 µM ($n = 3$ per concentration). The assay was started upon the addition of ATP to a final concentration of 5 mM, and absorbance read at 340 nm in a Synergy H1 multi-mode plate reader (BioTek, Winooski, VT, USA).

Culture of human iPSC-derived cardiomyocytes. We used cryopreserved human iPSC-derived cardiomyocytes (iCell Cardiomyocytes^2 FUJIFILM Cellular Dynamics, Madison, WI, USA). The cells were thawed and plated on custom-made 96-well or 6 well plates with inserts of polydimethylsiloxane (PDMS). PDMS vulcanized silicone transparent sheeting was obtained from SMI (Specialty Manufacturing, Inc, Saginaw, MI, USA) with 40D (D, Durometer or ≈ 1000 kPa) hardness and coverslips were cut out to fit in each well of 96 well or 6 well plates. PDMS coverslips were manually added to each well of 96/6 well plates (ThermoFisher Scientific, Waltham, MA USA) and each plate was subsequently sterilized. PDMS coverslips were then coated with Matrigel (500 µg/mL; BD Biosciences, San Jose, CA) before plating human iPSC-derived cardiomyocytes. 50,000 (96-well format for efficacy screening) or 200,000 cells (6-well format used for drug-induced cardiotoxicity screening) were thawed, plated per well, and allowed to form functional syncytia. Cells were maintained in RPMI (ThermoFisher Scientific, Waltham, MA USA) media supplemented with B27 + (ThermoFisher Scientific, Waltham, MA USA). Cardiomyocyte functional syncytia were maintained in culture for 7–10 days at 37 °C, in 5% CO_2 before the screening assays.

Expression of Ca^{2+}-handling proteins in human iPSC-derived cardiomyocytes using Western Blotting. Cells from the 96 well plates were collected using 2 × Laemmli sample buffer (Bio-Rad, Hercules, CA USA), 30 µL per well, and stored at − 20 °C. Samples were loaded into 4–20% Tris–Glycine polyacrylamide precast gels (ThermoFisher Scientific, Waltham, MA USA) and electrophoresis was carried out. The SDS-PAGE resolved proteins were transferred to iBlot stacks with regular PVDF membranes using the iBlot 2 Dry Blotting System (ThermoFisher Scientific, Waltham, MA USA). Nonspecific binding sites were blocked with 5% nonfat dry milk in PBS-T (in mmol/L, 3 KH_2PO_4, 10 Na_2HPO_4, 150 NaCl, 0.15% Tween 20, pH 7.2–7.4) for 30 min at room temperature. Membranes were then incubated with specific primary antibodies (Supplementary Table S1) diluted in 5% bovine serum albumin in PBS-T overnight at 4 °C. After washing 3 times for 10 min, membranes were incubated with horseradish peroxidase-conjugated secondary antibodies (Supplementary Table S1) diluted in 5% bovine serum albumin in PBS-T. After washing 3 times for 10 min, protein-antibody reactions were detected using Pierce SuperSignal Chemiluminescent Substrates (ThermoFisher Scientific, Waltham, MA USA). Detection and quantification of protein bands were performed with a Bio-Rad ChemiDoc system and Image Lab software 5 (Bio-Rad, Hercules, CA USA).

High-resolution optical mapping experiments in human iPSC-derived cardiac cells. We evaluated the effects of SERCA2a activators CDN1163, CP-154526, and Ro 41-0960 (Sigma-Aldrich, St Louis, MO, USA) using cryopreserved human iPSC-derived cardiomyocytes (iCell^2 cardiomyocytes, FUJIFILM Cellular Dynamics, Madison, WI, USA). Cardiomyocyte functional syncytia were loaded with the Ca^{2+}-sensitive dye Rhod-2 (ThermoFisher Scientific, Waltham, MA USA) to quantify compound effects on intracellular calcium flux, or with the voltage-sensitive dye FluVolt (ThermoFisher Scientific, Waltham, MA USA) to quantify changes in the membrane potential of iPSC-derived cardiac cells[65]. Small molecules were solubilized in DMSO at a stock concentration of 10 mM. The stock concentrations of the molecules were diluted in medium to 10× the final concentration for the assay. Baseline optical mapping data was collected before drug treatment. Following, 96-well drug delivery plates were treated with the compounds diluted in Hank's balanced salt solution (SAFC Biosciences, Lenexa, KS, USA) for 30 min before data acquisition. The plate was then positioned below a high-speed CCD camera (200 fps, 80 × 80 pixels) on a heating block to enable recording at physiological temperature (37 °C). Each 96-well plate was imaged using a validated LED illumination system that enables rapid acquisition of concentration–response data in a high-throughput fashion[37]. Based on the available in situ EC_{50} data acquired in this study, we tested CDN1163 and CP-154526 for stimulation of intracellular Ca^{2+} dynamics on a 96-format well at compound concentrations of 0.1, 0.5, 1, 5, 10, and 50 µM ($n = 6$ per concentration), and Ro 41-0960 at compound concentrations of 0.5, 1, 5, 10, 50, and 100 µM ($n = 6$ per concentration). Additionally, isoproterenol at a concentration of 1 µM was used as a positive control. We also evaluated the effects of CDN1163 on conduction velocity and APD_{90} on a 6-well plate format at compound concentrations of 0.5, 5, and 50 µM ($n = 6$ per concentration) to screen for potential cardiac toxicity effects induced by this molecule[37,66]. In all cases, data acquisition occurred before (baseline) and after treatment of cells with the compounds. Post-acquisition data analysis of human iPSC-derived cardiomyocyte screening assays was done using custom software[67,68].

Received: 22 February 2021; Accepted: 6 August 2021
Published online: 16 August 2021

References

1. Cournia, Z. *et al.* Membrane protein structure, function, and dynamics: A perspective from experiments and theory. *J. Membr. Biol.* **248**, 611–640. https://doi.org/10.1007/s00232-015-9802-0 (2015).
2. Muller, D. J., Wu, N. & Palczewski, K. Vertebrate membrane proteins: Structure, function, and insights from biophysical approaches. *Pharmacol. Rev.* **60**, 43–78. https://doi.org/10.1124/pr.107.07111 (2008).
3. Almen, M. S., Nordstrom, K. J., Fredriksson, R. & Schioth, H. B. Mapping the human membrane proteome: A majority of the human membrane proteins can be classified according to function and evolutionary origin. *BMC Biol.* **7**, 50. https://doi.org/10.1186/1741-7007-7-50 (2009).
4. Overington, J. P., Al-Lazikani, B. & Hopkins, A. L. Opinion—How many drug targets are there?. *Nat. Rev. Drug Discov.* **5**, 993–996. https://doi.org/10.1038/nrd2199 (2006).
5. Cheng, A. C. *et al.* Structure-based maximal affinity model predicts small-molecule druggability. *Nat. Biotechnol.* **25**, 71–75. https://doi.org/10.1038/nbt1273 (2007).
6. Yin, H. & Flynn, A. D. Drugging membrane protein interactions. *Annu. Rev. Biomed. Eng.* **18**, 51–76. https://doi.org/10.1146/annurev-bioeng-092115-025322 (2016).
7. Sudhahar, C. G., Haney, R. M., Xue, Y. & Stahelin, R. V. Cellular membranes and lipid-binding domains as attractive targets for drug development. *Curr. Drug Targets* **9**, 603–613. https://doi.org/10.2174/138945008785132420 (2008).
8. Yin, H. Exogenous agents that target transmembrane domains of proteins. *Angew. Chem. Int. Ed. Engl.* **47**, 2744–2752. https://doi.org/10.1002/anie.200704780 (2008).
9. Periasamy, M. & Huke, S. SERCA pump level is a critical determinant of Ca(2+)homeostasis and cardiac contractility. *J. Mol. Cell. Cardiol.* **33**, 1053–1063. https://doi.org/10.1006/jmcc.2001.1366 (2001).
10. Minamisawa, S. *et al.* Chronic phospholamban-sarcoplasmic reticulum calcium ATPase interaction is the critical calcium cycling defect in dilated cardiomyopathy. *Cell* **99**, 313–322 (1999).
11. Meyer, M. *et al.* A recombinant antibody increases cardiac contractility by mimicking phospholamban phosphorylation. *FASEB J.* **18**, 1312–1314 (2004).
12. Hoshijima, M. *et al.* Chronic suppression of heart-failure progression by a pseudophosphorylated mutant of phospholamban via in vivo cardiac rAAV gene delivery. *Nat. Med.* **8**, 864–871 (2002).
13. Makarewich, C. A. *et al.* The DWORF micropeptide enhances contractility and prevents heart failure in a mouse model of dilated cardiomyopathy. *Elife* https://doi.org/10.7554/eLife.38319 (2018).
14. Aguayo-Ortiz, R. & Espinoza-Fonseca, L. M. Linking biochemical and structural states of SERCA: Achievements, challenges, and new opportunities. *Int. J. Mol. Sci.* https://doi.org/10.3390/ijms21114146 (2020).
15. Fisher, M. E. *et al.* Dwarf open reading frame (DWORF) is a direct activator of the sarcoplasmic reticulum calcium pump SERCA. *Elife* https://doi.org/10.7554/eLife.65545 (2021).
16. Stroik, D. R. *et al.* Targeting protein-protein interactions for therapeutic discovery via FRET-based high-throughput screening in living cells. *Sci. Rep.* **8**, 12560. https://doi.org/10.1038/s41598-018-29685-z (2018).
17. Kaye, D. M., Hoshijima, M. & Chien, K. R. Reversing advanced heart failure by targeting Ca^{2+} cycling. *Annu. Rev. Med.* **59**, 13–28 (2008).
18. Hajjar, R. J. *et al.* Design of a phase 1/2 trial of intracoronary administration of AAV1/SERCA2a in patients with heart failure. *J. Card. Fail.* **14**, 355–367 (2008).
19. Yatime, L. *et al.* P-type ATPases as drug targets: Tools for medicine and science. *BBA Bioenerg.* **1787**, 207–220. https://doi.org/10.1016/j.bbabio.2008.12.019 (2009).
20. Tadini-Buoninsegni, F., Smeazzetto, S., Gualdani, R. & Moncelli, M. R. Drug interactions with the Ca^{2+}-ATPase from Sarco(Endo) Plasmic Reticulum (SERCA). *Front. Mol. Biosci.* https://doi.org/10.3389/fmolb.2018.00036 (2018).
21. Peetla, C., Stine, A. & Labhasetwar, V. Biophysical interactions with model lipid membranes: Applications in drug discovery and drug delivery. *Mol. Pharm.* **6**, 1264–1276. https://doi.org/10.1021/mp9000662 (2009).
22. Seddon, A. M. *et al.* Drug interactions with lipid membranes. *Chem. Soc. Rev.* **38**, 2509–2519. https://doi.org/10.1039/b813853m (2009).
23. Yu, H. B., Li, M., Wang, W. P. & Wang, X. L. High throughput screening technologies for ion channels. *Acta Pharmacol. Sin.* **37**, 34–43. https://doi.org/10.1038/aps.2015.108 (2016).
24. Lundstrom, K. Structural genomics and drug discovery. *J. Cell Mol. Med.* **11**, 224–238. https://doi.org/10.1111/j.1582-4934.2007.00028.x (2007).
25. Kang, S. *et al.* Small molecular allosteric activator of the sarco/endoplasmic reticulum Ca^{2+}-ATPase (SERCA) attenuates diabetes and metabolic disorders. *J. Biol. Chem.* **291**, 5185–5198. https://doi.org/10.1074/jbc.M115.705012 (2016).
26. Baker, J. E., LaConte, L. E., Thomas, D. D. & Brust-Mascher, I. Muscle chemistry and force. *Biophys. J.* **79**, 1687–1688 (2000).
27. Steenbergen, C., Deleeuw, G., Rich, T. & Williamson, J. R. Effects of acidosis and ischemia on contractility and intracellular pH of rat heart. *Circ. Res.* **41**, 849–858. https://doi.org/10.1161/01.res.41.6.849 (1977).
28. https://disco.chemaxon.com/calculators/reports/CHEMBL26-AZ_bpka_Eq_T_Report.html. Accessed 02 Aug 2021.
29. Postila, P. A., Vattulainen, I. & Rog, T. Selective effect of cell membrane on synaptic neurotransmission. *Sci. Rep.* **6**, 19345. https://doi.org/10.1038/srep19345 (2016).
30. Lyon, A. R. *et al.* SERCA2a gene transfer decreases sarcoplasmic reticulum calcium leak and reduces ventricular arrhythmias in a model of chronic heart failure. *Circ. Arrhythm Electrophysiol.* **4**, 362–372. https://doi.org/10.1161/CIRCEP.110.961615 (2011).
31. Liu, G. *et al.* Mechanism of adrenergic CaV1.2 stimulation revealed by proximity proteomics. *Nature* **577**, 695–700. https://doi.org/10.1038/s41586-020-1947-z (2020).
32. del Monte, F. *et al.* Restoration of contractile function in isolated cardiomyocytes from failing human hearts by gene transfer of SERCA2a. *Circulation* **100**, 2308–2311. https://doi.org/10.1161/01.cir.100.23.2308 (1999).
33. Seymour, P. A., Schmidt, A. W. & Schulz, D. W. The pharmacology of CP-154,526, a non-peptide antagonist of the CRH1 receptor: A review. *CNS Drug Rev.* **9**, 57–96. https://doi.org/10.1111/j.1527-3458.2003.tb00244.x (2003).
34. Hohendanner, F., McCulloch, A. D., Blatter, L. A. & Michailova, A. P. Calcium and IP3 dynamics in cardiac myocytes: Experimental and computational perspectives and approaches. *Front. Pharmacol.* **5**, 35. https://doi.org/10.3389/fphar.2014.00035 (2014).
35. Lipskaia, L., Chemaly, E. R., Hadri, L., Lompre, A. M. & Hajjar, R. J. Sarcoplasmic reticulum Ca(2+) ATPase as a therapeutic target for heart failure. *Expert Opin. Biol. Ther.* **10**, 29–41. https://doi.org/10.1517/14712590903321462 (2010).
36. Teneggi, V., Sivakumar, N., Chen, D. & Matter, A. Drugs' development in acute heart failure: What went wrong?. *Heart Fail. Rev.* https://doi.org/10.1007/s10741-018-9707-y (2018).
37. da Rocha, A. M., Creech, J., Thonn, E., Mironov, S. & Herron, T. J. Detection of drug-induced torsades de pointes arrhythmia mechanisms using hiPSC-CM syncytial monolayers in a high-throughput screening voltage sensitive dye assay. *Toxicol. Sci.* **173**, 402–415. https://doi.org/10.1093/toxsci/kfz235 (2020).
38. Johnson, D. M. & Antoons, G. Arrhythmogenic mechanisms in heart failure: Linking beta-adrenergic stimulation, stretch, and calcium. *Front. Physiol.* **9**, 1453. https://doi.org/10.3389/fphys.2018.01453 (2018).
39. King, J. H., Huang, C. L. & Fraser, J. A. Determinants of myocardial conduction velocity: Implications for arrhythmogenesis. *Front. Physiol.* **4**, 154. https://doi.org/10.3389/fphys.2013.00154 (2013).

40. Qu, Y. *et al.* Action potential recording and pro-arrhythmia risk analysis in human ventricular trabeculae. *Front. Physiol.* **8**, 1109. https://doi.org/10.3389/fphys.2017.01109 (2017).
41. Fernandez-Tenorio, M. & Niggli, E. Stabilization of Ca(2+) signaling in cardiac muscle by stimulation of SERCA. *J. Mol. Cell. Cardiol.* **119**, 87–95. https://doi.org/10.1016/j.yjmcc.2018.04.015 (2018).
42. Corbett, J. L. & Duncan, S. A. iPSC-derived hepatocytes as a platform for disease modeling and drug discovery. *Front. Med. Lausanne.* https://doi.org/10.3389/fmed.2019.00265 (2019).
43. Farkhondeh, A. *et al.* Induced pluripotent stem cells for neural drug discovery. *Drug Discov. Today* **24**, 992–999. https://doi.org/10.1016/j.drudis.2019.01.007 (2019).
44. Yue, Z., Li, C., Voth, G. A. & Swanson, J. M. J. Dynamic protonation dramatically affects the membrane permeability of drug-like molecules. *J. Am. Chem. Soc.* **141**, 13421–13433. https://doi.org/10.1021/jacs.9b04387 (2019).
45. Berben, P. *et al.* Drug permeability profiling using cell-free permeation tools: Overview and applications. *Eur. J. Pharm. Sci.* **119**, 219–233. https://doi.org/10.1016/j.ejps.2018.04.016 (2018).
46. Mateus, A. *et al.* Intracellular drug bioavailability: A new predictor of system dependent drug disposition. *Sci. Rep.* **7**, 43047. https://doi.org/10.1038/srep43047 (2017).
47. Paik, D. T., Chandy, M. & Wu, J. C. Patient and disease-specific induced pluripotent stem cells for discovery of personalized cardiovascular drugs and therapeutics. *Pharmacol. Rev.* **72**, 320–342. https://doi.org/10.1124/pr.116.013003 (2020).
48. Kim, S. *et al.* PubChem substance and compound databases. *Nucleic Acids Res.* **44**, D1202-1213. https://doi.org/10.1093/nar/gkv951 (2016).
49. O'Boyle, N. M. *et al.* Open Babel: An open chemical toolbox. *J. Cheminform.* **3**, 33. https://doi.org/10.1186/1758-2946-3-33 (2011).
50. Swain, M. chemicalize.org. *J. Chem. Inf. Model.* **52**, 613–615 (2012).
51. Pence, H. E. & Williams, A. Chemspider: An online chemical information resource. *J. Chem. Educ.* **87**, 1123–1124 (2010).
52. Lomize, A. L. *et al.* PerMM: A web tool and database for analysis of passive membrane permeability and translocation pathways of bioactive molecules. *J. Chem. Inf. Model* **59**, 3094–3099. https://doi.org/10.1021/acs.jcim.9b00225 (2019).
53. Lindorff-Larsen, K. *et al.* Improved side-chain torsion potentials for the Amber ff99SB protein force field. *Proteins* **78**, 1950–1958. https://doi.org/10.1002/prot.22711 (2010).
54. Abraham, M. J. *et al.* GROMACS: High performance molecular simulations through multi-level parallelism from laptops to supercomputers. *SoftwareX* **1–2**, 19–25 (2015).
55. Fiehn, W., Peter, J. B., Mead, J. F. & Gan-Elepano, M. Lipids and fatty acids of sarcolemma, sarcoplasmic reticulum, and mitochondria from rat skeletal muscle. *J. Biol. Chem.* **246**, 5617–5620 (1971).
56. Bick, R. J., Buja, L. M., Van Winkle, W. B. & Taffet, G. E. Membrane asymmetry in isolated canine cardiac sarcoplasmic reticulum: Comparison with skeletal muscle sarcoplasmic reticulum. *J. Membr. Biol.* **164**, 169–175. https://doi.org/10.1007/s002329900402 (1998).
57. Sousa da Silva, A. W. & Vranken, W. F. ACPYPE—AnteChamber PYthon Parser interfacE. *BMC Res. Notes* **5**, 367. https://doi.org/10.1186/1756-0500-5-367 (2012).
58. Jambeck, J. P. & Lyubartsev, A. P. An extension and further validation of an all-atomistic force field for biological membranes. *J. Chem. Theory Comput.* **8**, 2938–2948. https://doi.org/10.1021/ct300342n (2012).
59. Braga, C. & Travis, K. P. A configurational temperature Nose-Hoover thermostat. *J. Chem. Phys.* **123**, 134101. https://doi.org/10.1063/1.2013227 (2005).
60. Parrinello, M. & Rahman, A. Polymorphic transitions in single crystals: A new molecular dynamics method. *J. Appl. Phys.* **52**, 7182–7190 (1981).
61. Kumar, S., Rosenberg, J. M., Bouzida, D., Swendsen, R. H. & Kollman, P. A. The weighted histogram analysis method for fre-energy calculations on biomolecules. I. The Method. *J. Comput. Chem.* **13**, 1011–1021 (1992).
62. Gowers, R. *et al.* MD analysis: A Python package for the rapid analysis of molecular dynamics simulations. In *Proceedings of the 15th Python in Science Conference*, 98–105. https://doi.org/10.25080/majora-629e541a-00e (2016).
63. Gnuplot 5.0: An interactive plotting program (2017).
64. The PyMOL Molecular Graphics System v. 1.7 (2010).
65. Lee, P. *et al.* Simultaneous voltage and calcium mapping of genetically purified human induced pluripotent stem cell-derived cardiac myocyte monolayers. *Circ. Res.* **110**, 1556–1563. https://doi.org/10.1161/CIRCRESAHA.111.262535 (2012).
66. Gintant, G. *et al.* Repolarization studies using human stem cell-derived cardiomyocytes: Validation studies and best practice recommendations. *Regul. Toxicol. Pharmacol.* **117**, 104756. https://doi.org/10.1016/j.yrtph.2020.104756 (2020).
67. Campbell, K. *et al.* Spatial gradients in action potential duration created by regional magnetofection of hERG are a substrate for wavebreak and turbulent propagation in cardiomyocyte monolayers. *J. Physiol.* **590**, 6363–6379. https://doi.org/10.1113/jphysiol.2012.238758 (2012).
68. da Rocha, A. M. *et al.* hiPSC-CM monolayer maturation state determines drug responsiveness in high throughput pro-arrhythmia screen. *Sci. Rep.* **7**, 13834. https://doi.org/10.1038/s41598-017-13590-y (2017).

Acknowledgements

This work was supported by the National Institutes of Health grants R01HL148068 (to L.M.E.-F. and T.J.H), R01GM120142 (to L.M.E.-F.) and R44ES027703 (to T.J.H), by a Michigan Drug Discovery Grant MDD2019202 (to L.M.E.F.), and by an American Heart Association Grant 19POST34380706 (to E.N.J.-V.). R. A.-O. thanks DGTIC-UNAM for the supercomputing resources and technical support (LANCAD-UNAM-DGTIC-398). This research was supported in part through computational resources and services provided by Advanced Research Computing at the University of Michigan, Ann Arbor, Michigan.

Author contributions

L.M.E.-F. and T.J.H. designed research; R.A.-O., J.C., E.N.J.-V., G.G.-S., N.W., and A.M. da R. performed research; R.A.-O., E.N.J.-V., G.G.-S., A.M. da R., T.J.H., and L.M.E.-F. analyzed data and interpreted results; L.M.E.-F. wrote the paper.

Competing interests

L.M.E.-F. is an editorial board member for *Scientific Reports*. T.J.H is co-founder of Cartox, Inc., and consultant to StemBioSys, Inc.

Additional information

Supplementary Information The online version contains supplementary material available at https://doi.org/10.1038/s41598-021-96217-7.

Correspondence and requests for materials should be addressed to L.M.E.-F.